Mansour, M. A.; Bakier, M. A. Y.

Article

Influence of thermal boundary conditions on MHD natural convection in square enclosure using Cu-water nanofluid

Energy Reports

Provided in Cooperation with:
Elsevier

Suggested Citation: Mansour, M. A.; Bakier, M. A. Y. (2015) : Influence of thermal boundary conditions on MHD natural convection in square enclosure using Cu-water nanofluid, Energy Reports, ISSN 2352-4847, Elsevier, Amsterdam, Vol. 1, pp. 134-144, https://doi.org/10.1016/j.egyr.2015.03.005

Energy Reports 1 (2015) 134–144

Contents lists available at ScienceDirect

Energy Reports

journal homepage: www.elsevier.com/locate/egyr

Influence of thermal boundary conditions on MHD natural convection in square enclosure using Cu–water nanofluid

M.A. Mansour, M.A.Y. Bakier *

Department of Mathematics, Faculty of Science, Assiut University, Assiut, Egypt

ARTICLE INFO

Article history:
Received 8 November 2014
Received in revised form
26 February 2015
Accepted 28 March 2015
Available online 6 June 2015

Keywords:
Magneto hydrodynamics
Nanofluid
Configurations
Inclination angle
Nusselt number

ABSTRACT

Numerical investigation for heat transfer with natural convection and nanofluid flow subjected to changeable thermal boundary conditions and inclined magnetic field has been performed. Effect of problem's parameters on each other has been monitored. It has been reached to that inclination angle can justify the quasi-symmetric boundary conditions to be symmetric. In addition to that as inclination angle increases, the magnetic force pointed to horizontal trend; so the convection regime dominates the cavity. In a related context, nanoparticles provide conduction regime, increase and maintenance the rate of heat transfer all over the cavity. However thermal emission at ends of heat source–sink has been found to be constant when boundary conditions change in the pure case.

1. Introduction

Considerable attention is given to the study of natural convection in enclosures which are filled with volumetric heat generating fluids. The application areas are in nuclear reactor design, post-accident heat removal in nuclear reactors, geophysics and underground storage of nuclear waste and play an important role as a dominating mechanism in energy conservation and energy efficient design in building enclosures, home heating and cooling. Natural convection besides its importance in such processes, due to the coupling of fluid flow and energy transport, the phenomenon of natural convection remains an interesting field of investigation, especially in conditioning air of habitat. In fact, the flow pattern and the representation of the thermal boundary conditions of a room surfaces have a direct effect upon the accuracy of predicting the thermal comfort, indoor air quality, heating and cooling loads for the room especially where large glazed surfaces are present.

M. Sheikholeslami and D.D. Ganji have found that choosing Titanium oxide as the nanoparticle and Ethylene glycol as base fluid proved to have the highest cooling performance for this problem. Fluid temperature increases due to increase in the thermal conductivity parameter, volume fraction of the nanoparticles while it decreases due to increase in the Velocity ratio parameter. The use of nanotubes (cylindrical shaped nanoparticles) in model *II* proved to have higher heat transfer enhancement as compared to spherical shaped nanoparticles (model *I*) (Sheikholeslami and Ganji, 2014). The results of M. Sheikholeslami, et al. have revealed that the enhancement in heat transfer increases as Hartmann number and heat source length increase but it decreases with increase of Rayleigh number. Also it can be found that effect of Hartmann number and heat source length is more pronounced at high Rayleigh number (Sheikholeslami et al., 2014). Also, M. Sheikholeslami et al. have shown that Nusselt number has direct relationship with nanoparticle volume fraction and Rayleigh number but it has inverse relationship with Hartmann number and position of inner cylinder at high Rayleigh number. Also it can be concluded that heat transfer enhancement increases with increase of Hartmann number and decreases with augment of Raleigh number (Sheikholeslami et al., 2014). In the same context, M. Sheikholeslami and D.D. Ganji have indicated that skin friction parameter increases with augment of Reynolds number and Rotation parameter but it decreases with increase of injection parameter. Also it can be found that Nusselt number has a direct relationship with Reynolds number and injection parameter while it has a reverse relationship with Rotation parameter, Schmidt number, Thermophoretic parameter and Brownian parameter (Sheikholeslami and Ganji, 2014). Results of M. Sheikholeslami, et al. proved that enhancement ratio increases with decrease of Rayleigh number and it increases with augment of Hartmann number. Also it can be concluded that Nusselt number has a direct relationship with nanoparticle volume fraction, Rayleigh number and it has a reverse relationship with Hartmann number (Sheikholeslami et al., 2014). M. Sheikholeslami and D.D. Ganji have indicated that skin

* Corresponding author. Tel.: +20 01118812917.
E-mail address: mohameda.yousof@gmail.com (M.A.Y. Bakier).

http://dx.doi.org/10.1016/j.egyr.2015.03.005

Nomenclature

B	heat source length
c_p	specific heat at constant pressure (J kg^{-1} K^{-1})
D	heat source location
g	acceleration due to gravity (m s^{-2})
H	height of cavity
Ha	Hartmann number $= \beta_0 W(\sigma/\mu)^{0.5}$
k	thermal conductivity (W m^{-1} K^{-1})
Nu_l	local Nusselt number
Nu_m	average Nusselt number
p	pressure of the fluid (N m^{-2})
Pr	Prandtl number
q_w	heat flux at the surface (W m^{-2})
Ra	Rayleigh number
T	temperature of the fluid (K)
u, v	dimensional velocity components along the (x, y) axes (m s^{-1})
x, y	axis in the direction along and normal to the tangent of the surface
ρ	density of the fluid (kg m^{-3})
θ	dimensionless temperature function
α	thermal diffusivity
μ	viscosity of the fluid (kg m^{-1} s^{-1})
ψ	Stream function
Φ	Inclination angle
β	volumetric coefficient of thermal expansion (K^{-1})
β_0	strength of the magnetic field (T)
ν	kinematic viscosity (m^2 s^{-1})
σ	electrical conductivity $((\Omega m)^{-1})$
φ	solid volume fraction

Subscripts

C	the minimum temperature
eff	effective value
f	fluid particle
H	the maximum temperature
i, j	positions in the grid
l	local value
m	mean value
nf	nanofluid property
s	solid particle or heat source

friction parameter increases with augment of Reynolds number, Rotation parameter and Magnetic parameter. Also it can be found that Nusselt number has a direct relationship with Reynolds number while it has a reverse relationship with Rotation parameter, Magnetic parameter, Schmidt number, Thermophoretic parameter and Brownian parameter (Sheikholeslami and Ganji, 2014). M. Sheikholeslami, et al. have revealed that average Nusselt number is an increasing function of nanoparticle volume fraction and Rayleigh number, while it is a decreasing function of Hartmann number. Moreover it can be found that the enhancement in heat transfer increases as Hartmann number increases but it decreases with increase of Rayleigh number (Sheikholeslami et al., 2013).

A study of natural convection in cavities heated from below by a thermal source which dissipated energy at a constant rate carried by Ramos and Milanez (1998). Sezai and Mohamad (2000) studied three-dimensional natural convection from a discrete flush-mounted rectangular heat source on the bottom of a horizontal enclosure. The upper wall surface was maintained at a cold temperature and two kinds of boundary conditions were applied on the sidewalls. A numerical study on natural convection in a glass-melting tank heated locally from below is due to Sarris et al. (2004). More recently, Calgagni et al. (2005) investigated an experimental and numerical study of free convective heat transfer in a square enclosure characterized by a discrete heater located on the lower wall and cooled from the lateral walls. A numerical investigation of natural convection of air in a vertical square cavity with localized isothermal heating from below and symmetrical cooling from the sidewalls was carried by Aydin and Yang (2000). The top wall as well as the non-heated parts of the bottom wall was considered adiabatic. Sharif and Mohammad (2005) studied the same configuration as Aydin and Yang, where the localized isothermal heat source at the bottom wall was replaced with a constant flux heat source. They investigated the effect of aspect ratio and inclination of the cavity on the heat transfer process.

Ben Cheikh et al. (2007) investigated natural convection in a square cavity heated locally from below with a constant flux source and cooled from above with several specified thermal boundary conditions at the top and sidewalls.

As the boundaries have great effect, the kind of medium and other external forces have the most dangerous effect on flow and heat patterns.

As a consequence, there has been increased interest in the flows of electrically conducting fluid in cavities subjected to external magnetic field. For an electrically conducting fluid exposed to a magnetic field, Lorentz force is also active and interacts with the buoyancy force in governing the flow and temperature fields. Rudraiah et al. (1995) investigated the effect of surface tension on buoyancy driven flow of an electrically conducting fluid in a square cavity in presence of a vertical transverse magnetic field to see how this force damps hydrodynamic movements, since, this is required to enhance crystal purity, increase compositional uniformity and reduce defect density. Al-Najem et al. (1998) used the power control volume approach to determine the flow and temperature fields under a transverse magnetic field in a titled square enclosure with isothermal vertical walls and adiabatic horizontal walls at Prandtl number of 0.71. They showed that the suppression effect of the magnetic field on convection currents and heat transfer is more significant for low inclination angles and high Grashof numbers. Ikezoe et al. (1998) have presented many interesting phenomena occurred in the magnetic field such as the levitation of a water droplet by strong magnetic field, and driving of air flow due to magnetic field. Wakayama (1991), Wakayama et al. (2001) and Wakayama and Wakayama (2001) found very interesting phenomena such as jet stream of nitrogen gas into air (Wakayama jet) in a steeply decreasing magnetic field, enhancement of combustion flames and sustaining flame under microgravity. El Jery et al. (2010) examine the influence of an external oriented magnetic field on entropy generation as well as on heat transfer and fluid flow in natural convection of two different fluids which are air (with $Pr = 0.71$) and liquid gallium (with $Pr = 0.02$) enclosed in a square cavity.

Macroscopic models for nanofluid flow and heat transfer can be classified as single-phase and two-phase models (Sarkar, 2011; Saidur et al., 2011; Heris et al., 2007). Single-phase approaches consider nanoparticles and base fluid as a single homogeneous fluid with respect to its effective properties (Maiga et al., 2004). While two-phase approaches handle continuity, momentum and energy equations for particles and base fluid using three different methods. One of these methods is Eulerian Mixture model (EMM) where momentum and energy equations are solved for mixture phase coupled with continuity equation for each phase, then phase velocities are related by empirical correlations (Lotfi et al., 2010; Ahmad et al., 2010). The other method is the Eulerian Eulerian model (EEM) where separate continuity, momentum, and energy equations for each phase are solved. This approach is suggested for flows where interactions between phases are not well defined (Kalteh et al., 2011). Although two-phase models

provide a better understanding of both phases, single-phase models are computationally more efficient, however provide less detail about each phase (Kalteh et al., 2011).

In this approach, the effect of nanoparticle-base fluid relative velocity is treated as a perturbation of the energy equation and an empirical dispersion coefficient is introduced to describe the heat transfer enhancement. Numerical formulation is developed using the single-phase model proposed by Xuan and Roetzel (2000) that accounts for thermal dispersion of nanoparticles in the base fluid. Skin friction coefficients increase with increase of squeeze number and Hartmann number but they decrease with augment of solid volume fraction. Nusselt number increases with increase of solid volume fraction and Hartmann number while it decreases with increase of squeeze number (Sheikholeslami and Ganji, 2015). Particles with a smaller size have better ability to dissipate heat, and a larger volume fraction would provide a stronger driving force which leads to increase in temperature profile. Nusselt number has direct relationship with the Rayleigh number and heat source length while it has reverse relationship with size of nanoparticle and volume fraction of cobalt (Sheikholeslami and Gorji-Bandpy, 2014). The average Nusselt number is an increasing function of nanoparticle volume fraction as well as the Rayleigh number, while it is a decreasing function of the Hartmann number (Sheikholeslami et al., 2012).

Magnetic nanofluid is a magnetic colloidal suspension of carried liquid and magnetic nanoparticles. The advantage of magnetic nanofluid is that fluid flow and heat transfer can be controlled by external magnetic field, which makes it applicable in various fields such as electronic packing, thermal engineering and aerospace. Sheikholeslami et al. (2014) has studied Al_2O_3 nanofluid flow in presence of magnetic field using LBM, they calculated the effective thermal conductivity (where the Brownian model was considered) and viscosity by KKL correlation. They found that Nusselt number is an increasing function of nanoparticle volume fraction and Rayleigh number but it is a decreasing function of Ha except for $Ra = 10^4$ where the pattern inverses around the critical value $Ha_c = 40$. He (Sheikholeslami, 2014) has used CVFEM to study ferrofluid flow and heat transfer in the presence of magnetic field. Nusselt number is an increasing function of magnetic number, Rayleigh number and solid volume fraction while it does conversely with Hartmann number. Also, heat transfer decreases with increase in both Ra and magnetic number but it increases with increase in Hartmann number.

For ferrofluid in semi annulus enclosure with considering of thermal radiation, Nusselt number is an increasing function of Ra, solid volume fraction and magnitude number, while it is a decreasing function with Hartmann number and radiation parameter (Sheikholeslami et al., 2014). Heat transfer rate and dimensionless entropy generation number increase with increase of Rayleigh number and solid volume fraction, but they decrease with increase of Hartmann number (Sheikholeslami and Ganji, 2015). M. Sheikholeslami, et al. have found that maximum stream value decreases with increase of Hartmann number. Augmentation of Ha causes Nu to decrease (Sheikholeslami et al., 2015). Magnitude of skin friction coefficient is an increasing function of magnitude number, rotation number, and Reynolds number but it is a decreasing function of solid volume fraction. Nusselt number increases with increase of volume fraction and Reynolds number but it decreases with Eckert number, magnitude number and rotation parameter (Sheikholeslami et al., 2014). M. Sheikholeslami and D.D. Ganji have studied effect of field on ferrofluid flow and heat transfer. Nusselt number increases with augmentation of Rayleigh number and solid volume fraction. But it decreases with increase of Hartmann number. At low Rayleigh number, heat transfer is an increasing function of magnitude number while for high Ra, it is vice versa (Sheikholeslami and Ganji, 2014). The results of Sheikholeslami et al. (2014) show that as Hartmann number increases Nusselt number decreases while opposite trend is observed as nanoparticles volume fraction, Rayleigh number and aspect ratio increase. Domination of conduction mechanism causes heat transfer enhancement to increase. So enhancement in heat transfer increases with increase of Hartmann number and aspect ratio while it decreases with augment of Rayleigh number. Nusselt number is an increasing function of buoyancy ratio number but it is a decreasing function of Lewis number and Hartmann number. Also it can be concluded that as buoyancy ratio number increases the effects of other active parameters are more pronounced (Sheikholeslami et al., 2014). In addition, Nusselt number is an increasing function of nanoparticles volume fraction, dimensionless amplitude of the sinusoidal wall and Rayleigh number while it is a decreasing function of Hartmann number (Sheikholeslami et al., 2014). Hamad (2011) analytically investigated the natural convection of a nanofluid over a linearly stretching sheet in the presence of a vertical magnetic field. He showed that for a given value of the solid concentration, the heat transfer rate decreases as magnetic field increases. The point in his work is that the effective value of the electric conductivity for nanofluid was not calculated and that in the governing equations the electric conductivity is set according to the properties of the base fluid. Thus the increase of the solid volume fraction, in a given magnetic field, does not affect the Lorenz force. Ghasemi et al. (2011) studied numerically the magnetic field effect on natural convection in a square enclosure filled by a nanofluid. They have used basic mixture model for calculation of effective electric conductivity of nanofluids. Their results showed that the effect of the solid volume fraction on the heat transfer rate strongly depends on the values of the Rayleigh and Hartmann numbers. Nemati et al. (2012) considered the effect of the magnetic field on natural convection of nanofluid by using Lattice Boltzmann model. Their results indicated that the averaged Nusselt number increased with increase of the solid volume fraction parameter, while in the presence of a high magnetic field, this effect is decreased. Mahmoudi et al. (2013) also, investigate the entropy generation and enhancement of heat transfer in natural convection flow and heat transfer using Cu–water nanofluid in the presence of a constant magnetic field. The analysis uses a two dimensional trapezoidal enclosure with the left vertical wall and inclined walls kept in a low constant temperature and a heat source with constant heat flux placed on the bottom wall of the enclosure (see Table 1).

2. Mathematical modeling

Considering two-dimensional laminar natural convection of incompressible nanofluids in square enclosure depicted in Figs. 1a and 1b. Now for the steady motion of the equations for conservation of mass, momentum and energy in rectangular coordinate systems are given by:

$$\frac{\partial u}{\partial x}+\frac{\partial v}{\partial y}=0 \tag{1}$$

$$u\frac{\partial u}{\partial x}+v\frac{\partial u}{\partial y} = -\frac{1}{\rho_{nf}}\frac{\partial p}{\partial x}+\nu_{nf}\left(\frac{\partial^2 u}{\partial x^2}+\frac{\partial^2 u}{\partial y^2}\right) + \frac{\sigma_{nf}B_0^2}{\rho_{nf}}(v\sin\Phi\cos\Phi-u\sin^2\Phi) \tag{2}$$

$$u\frac{\partial v}{\partial x}+v\frac{\partial v}{\partial y} = -\frac{1}{\rho_{nf}}\frac{\partial p}{\partial y}+\nu_{nf}\left(\frac{\partial^2 v}{\partial x^2}+\frac{\partial^2 v}{\partial y^2}\right) + \frac{\sigma_{nf}B_0^2}{\rho_{nf}}(u\sin\Phi\cos\Phi-v\cos^2\Phi) + \frac{(\rho\beta)_{nf}}{\rho_{nf}}g(T-T_c) \tag{3}$$

$$u\frac{\partial T}{\partial x}+v\frac{\partial T}{\partial y}=\alpha_{nf}\left(\frac{\partial^2 T}{\partial x^2}+\frac{\partial^2 T}{\partial y^2}\right). \tag{4}$$

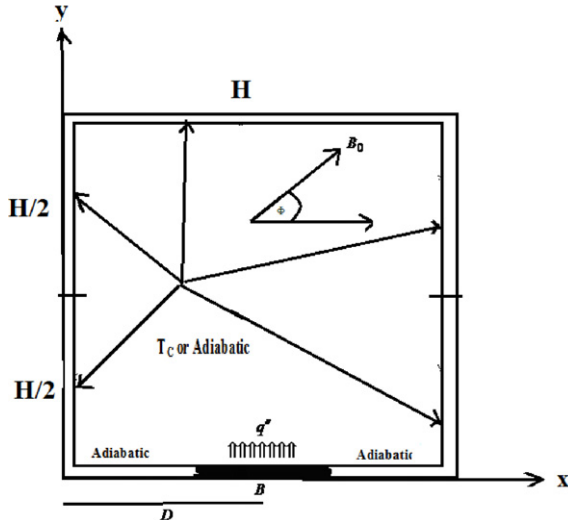

Fig. 1a. Sketch of the geometry and coordinate system of the cavity.

Table 1
Thermophysical properties of water and copper.

Property	Water	Copper (Cu)
ρ	997.1	8933
C_p	4179	385
k	0.613	401
β	21×10^{-5}	1.67×10^{-5}
σ	0.05	5.96×10^{7}

In Eqs. (1)–(4), x and y are Cartesian coordinates measured along the horizontal and vertical walls of the cavity respectively, u and v are the velocity components along the x- and y-axes respectively, T is the fluid temperature, p is the fluid pressure, g is the gravity acceleration.

Numerous formulations for the thermo-physical properties of nanofluids are proposed in the literature (Table 1). In the present study, we are adopting the relations which depend on the nanoparticles volume fraction only and which were proven and used in many previous studies (Einstein, 1956; Brinkman, 1952) as follows:

The effective density of the nanofluid is given as:

$$\rho_{nf} = (1-\phi)\rho_f + \phi\rho_p \tag{5}$$

where ϕ is the solid volume fraction of the nanofluid, ρ_f and ρ_p are the densities of the fluid and of the solid fractions respectively, and the heat capacitance of the nanofluid given is by Khanafer et al. (2003) as,

$$(\rho c_p)_{nf} = (1-\phi)(\rho c_p)_f + \phi(\rho c_p)_p. \tag{6}$$

The thermal expansion coefficient of the nanofluid can be determined by:

$$(\rho\beta)_{nf} = (1-\phi)(\rho\beta)_f + \phi(\rho\beta)_p \tag{7}$$

where β_f and β_p are the coefficients of thermal expansion of the fluid and of the solid fractions respectively.

Thermal diffusivity, α_{nf} of the nanofluid is defined by Oztop and Abu-Nada (2008) as:

$$\alpha_{nf} = \frac{k_{nf}}{(\rho c_p)_{nf}}. \tag{8}$$

In Eq. (8), k_{nf} is the thermal conductivity of the nanofluid which for spherical nanoparticles, according to the Maxwell–Garnett model (Maxwell, 1904), is:

$$\frac{k_{nf}}{k_f} = \frac{(k_p + 2k_f) - 2\phi(k_f - k_p)}{(k_p + 2k_f) + \phi(k_f - kp)}. \tag{9}$$

The effective dynamic viscosity of the nanofluid based on the Brinkman model (Brinkman, 1952) is given by

$$\mu_{nf} = \frac{\mu_f}{(1-\phi)^{2.5}} \tag{10}$$

where μ_f is the viscosity of the fluid fraction and the effective electrical conductivity of nanofluid was presented by Maxwell (1904) as

$$\frac{\sigma_{nf}}{\sigma_f} = 1 + \frac{3(\gamma-1)\phi}{(\gamma+2) - (\gamma-1)\phi} \tag{11}$$

where $\gamma = \frac{\sigma_p}{\sigma_f}$.

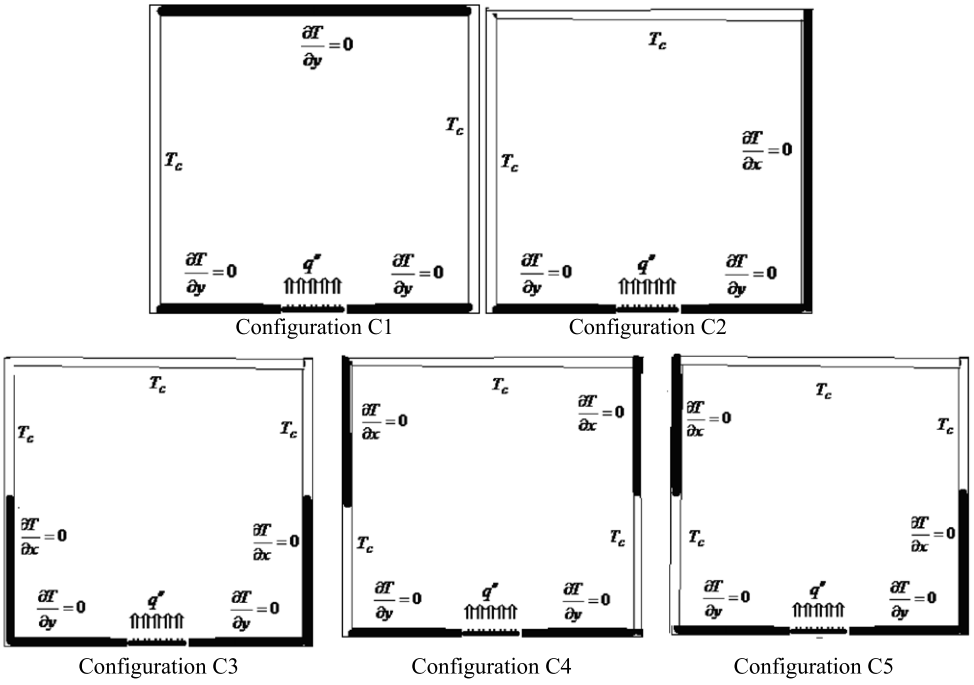

Fig. 1b. Thermal configurations of the cavity.

Introducing the following dimensionless set:

$$X = \frac{x}{H}, \qquad Y = \frac{y}{H}, \qquad U = \frac{uH}{\alpha_f},$$
$$V = \frac{vH}{\alpha_f}, \qquad P = \frac{pH^2}{\rho_{nf}\alpha_f^2}, \tag{12}$$
$$\theta = \frac{T - T_c}{\Delta T}, \qquad \tau = \frac{\alpha_f}{H^2}t, \qquad \Delta T = (T_h - T_c)$$

into Eqs. (1)–(4) yields the following dimensionless equations:

$$\frac{\partial U}{\partial X} + \frac{\partial V}{\partial Y} = 0 \tag{13}$$

$$U\frac{\partial U}{\partial X} + V\frac{\partial U}{\partial Y} = -\frac{\partial P}{\partial X} + \frac{\mu_{nf}}{\rho_{nf}\alpha_f}\left(\frac{\partial^2 U}{\partial X^2} + \frac{\partial^2 U}{\partial Y^2}\right) + Ha^2 \cdot Pr \cdot \frac{\sigma_{nf}}{\sigma_f} \cdot \frac{\beta_f}{\rho_{nf}} \cdot (V \sin\Phi \cos\Phi - U \sin^2\Phi) \tag{14}$$

$$U\frac{\partial V}{\partial X} + V\frac{\partial V}{\partial Y} = -\frac{\partial P}{\partial Y} + \frac{\mu_{nf}}{\rho_{nf}\alpha_f}\left(\frac{\partial^2 V}{\partial X^2} + \frac{\partial^2 V}{\partial Y^2}\right) + Ha^2 \cdot Pr \cdot \frac{\sigma_{nf}}{\sigma_f} \cdot \frac{\beta_f}{\rho_{nf}} \cdot (U \sin\Phi \cos\Phi - V \cos^2\Phi) + \frac{(\rho\beta)_{nf}}{\rho_{nf}\beta_f} \cdot Ra \cdot Pr \cdot \theta \tag{15}$$

$$U\frac{\partial \theta}{\partial X} + V\frac{\partial \theta}{\partial Y} = \frac{\alpha_{nf}}{\alpha_f}\left(\frac{\partial^2 \theta}{\partial X^2} + \frac{\partial^2 \theta}{\partial Y^2}\right) \tag{16}$$

where $Pr = \frac{\nu_f}{\alpha_f}$, $Ra = \frac{g\beta_f \Delta T H^3}{\nu_f \alpha_f}$, $Ha = B_0 H\sqrt{\frac{\sigma_f}{\mu_f}}$ are respectively the Prandtl number, the Rayleigh number and the Hartmann number.

The enclosure boundary conditions consist of no-slip and no-penetration walls, i.e. $u = v = 0$ on all four walls. The thermal boundary conditions assumed are $\theta = 0$ or $\partial\theta/\partial n = 0$ at any cooled or adiabatic sidewalls, respectively. Here, n is the unit normal to the boundary surface. On the bottom wall the boundary conditions are as follows:

$$\frac{\partial \theta}{\partial Y} = \begin{cases} 0 & \text{for } 0 \le X \le D - B/2 \\ -\frac{k_{nf}}{k_f} & \text{for } D - B/2 \le X \le D + B/2 \\ 0 & \text{for } D + B/2 \prec X \prec 1. \end{cases} \tag{17}$$

The local Nusselt number is defined as:

$$Nu_s = \frac{1}{\theta_s(X)}. \tag{18}$$

And the average Nusselt number is defined as:

$$Nu_m = \frac{1}{B}\int_{D-0.5*B}^{D+0.5*B} Nu_s dX. \tag{19}$$

3. Numerical procedure

The set of governing equations is numerically solved by the finite difference method. The governing equations are solved line by line by employing the ADI method, whereas the stream function equation is solved point by point. The finite difference form of diffusion and convection terms are written based on three points central difference which has second order accuracy. To check the convergence of the sequential iterative solution, the sum of the absolute differences of the solution variables between two successive iterations has been calculated. When this summation falls below the convergence criterion, convergence is obtained, which the convergence criterion has been chosen as 10^{-7}. To allow grid independent examination, the numerical procedure has been conducted for different grid resolutions. This method was found to be suitable and gave results that are very close to the numerical results obtained by Haajizadeh et al. (1984) and Grosan et al. (2009) for classical fluid. As we can see from Table 2 the present results give a good agreement with the results obtained by the authors mentioned above. These favorable comparisons lend confidence in the numerical results to be reported subsequently. The obtained results for both θ_{max} and ψ_{max} provide good accuracy (to some extent) to the numerical method. As shown in Table 2 the computed values are stable with respect to the Rayleigh number parameter, so the accuracy of FDM method is independent of *Ra*.

Table 2
Numerical comparisons for various Ra numbers.

Ra	Haajizadeh et al. (1984)		Grosan et al. (2009)		Present method	
	ψ_{max}	θ_{max}	ψ_{max}	θ_{max}	ψ_{max}	θ_{max}
10	0.078	0.130	0.079	0.127	0.0799	0.1272
10^3	4.880	0.118	4.833	0.116	4.8266	0.117

4. Discussion of results

Numerical simulations are performed for fluid flow and thermal characteristics associated with the natural convection heat transfer in enclosure filled with Cu–water nanofluid containing pair heat source–sink placed in the horizontal walls is studied. The parameters considered in the present study are length of heat source ($0.2 < B < 0.8$), heat source location ($0.3 < D < 0.7$), Hartmann number ($0 < Ha < 100$), solid volume fraction ($0 < \varphi < 0.2$), inclination angle ($0^0 < \Phi < 90^0$), Rayleigh number ($10^3 < Ra < 10^5$), and $Pr = 6.2$. The observations are reported as follows:

(a) The effect of thermal boundary changing, nanoparticles and inclination angle.

Fluid flow is symmetric around a vertical centerline in $C1$, where two circulating cells are formed; one in the clockwise direction then the other will be in the inverse to hold continuity equation for all fluid particles. Stream function increases as position closes to the core of circulating cell. The motion's forces are the buoyancy, viscous and the magnetic forces, magnetic force suppresses the convection regime resulted in buoyancy force. As inclination angle increases, the magnetic force pointed to horizontal trend; so the convection regime dominates the cavity and the flow in the left half greater than the other which is noticed from results (Fig. 2a). Stream values decrease for nanofluid due to the heterogeneity of the particles. $C2$ configuration rises stream values and vanishes the symmetry. Vertical velocity increases near to bottom and top surfaces, while the horizontal is greatest in the middle region. Increase of inclination angle positively affects the flow up to $\pi/4$. But stream changes qualitatively at $\pi/2$ where quasi-symmetry has been occurred around the vertical line adjacent to centerline. It is construed by two reasons; the horizontal velocity resultant of convection regime increases as position closes to side walls while the magnetic force works at the inversion direction of U diffusion for each particle. Therefore the velocity vanishes (stream function vanishes) at some point on each horizontal line intersect the cavity. The group of these points form symmetric axis that is seen in Fig. 2a. The domination of the left circulating cell is due to the nature of the magnetic work. Generally, magnetic field does not play role except for supplement the left half than the other as observed in $\pi/4$, $\pi/2$. Although the shape in $C4$ can be divided into two halves, there is no symmetry for stream. So the insulated parts in this configuration are not effective. The symmetry at $\Phi = \pi/2$ is construed as the magnetic force divides

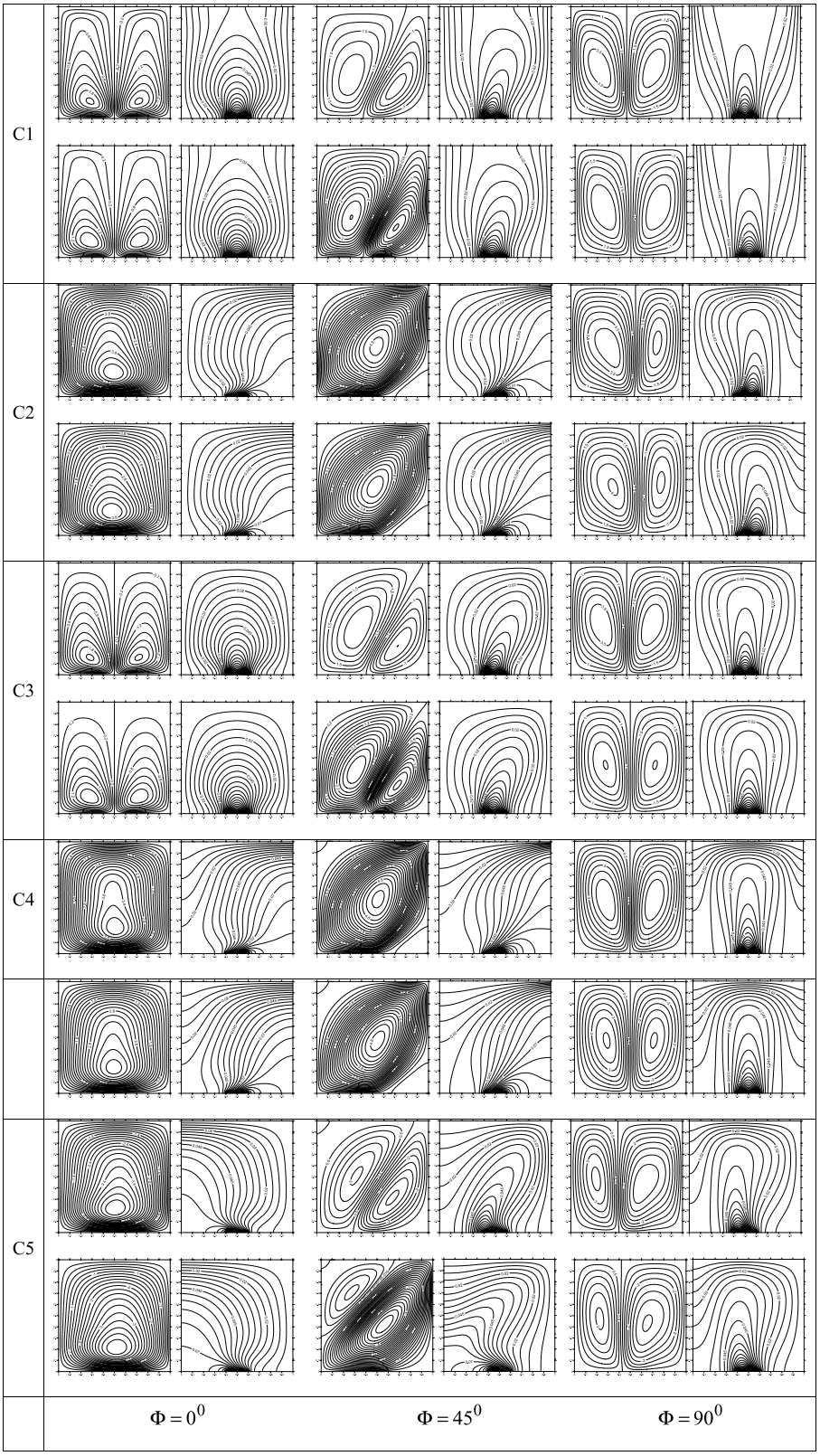

Fig. 2a. Streamlines (left) and Isotherms (right) for $\phi = 0.05$ (top) and $\phi = 0.05$ (bottom) at $Ha = 50,\ D = 0.5, B = 0.2$.

the resultant force into two parts, so all cases of this position are symmetry. The flow trend in $C5$ is unidirectional. The trend of motion is inverse $C2$ and $C4$ because $C5$ differs from them in the high-half of left side. There is not symmetry for the asymmetric thermal conditions. As angle increases, magnetic force divides the buoyancy force into two parts. Since the boundary conditions are reciprocal, two circulating cells differ in trend can be formed. This is clearly noticed at $\Phi = \pi/2$ so this parameter can justify the quasi-symmetric boundary conditions to be symmetric.

Conduction regime in $C1$ dominates the cavity because of the distribution of thermal conditions and magnetic field. Existence of adiabatic surfaces in the top helps to transfer temperature all

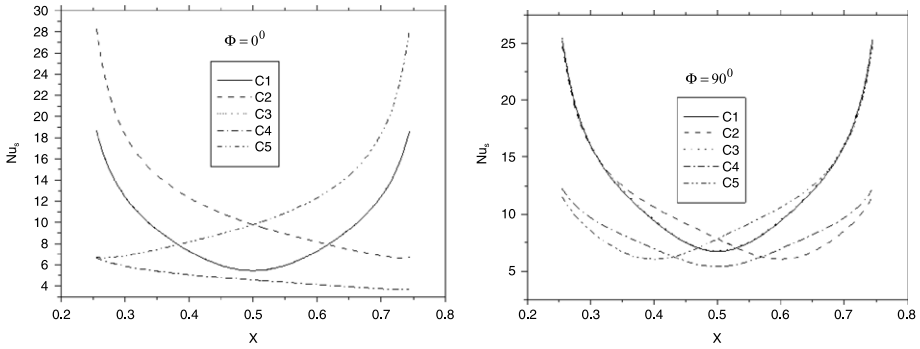

Fig. 2b. Profiles of the Local Nusselt number along the heat source at $\phi = 0.05$, $Ra = 10^6$, $Ha = 50$, $D = 0.5$, $B = 0.5$.

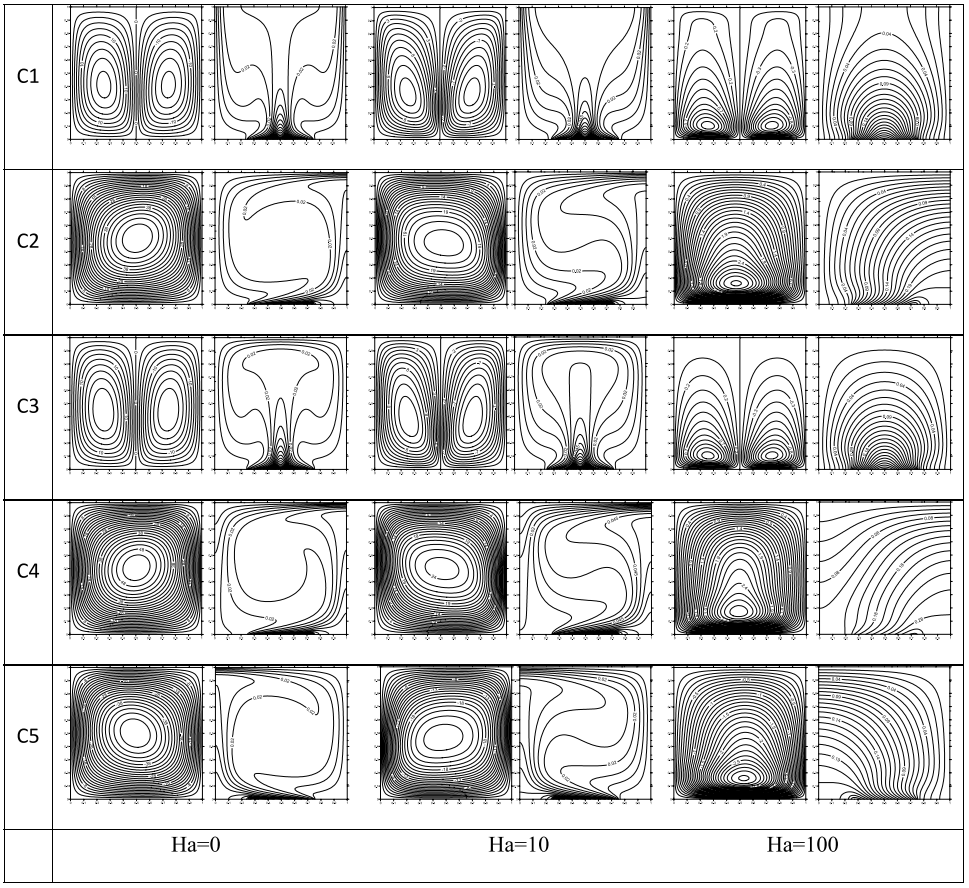

Fig. 3a. Streamlines(left) and Isothermal(right) at $\phi = 0.05$, $Ra = 10^6$, $D = 0.5$, $B = 0.5$, $\Phi = 0^0$.

over the cavity. As angle increases, the convection regime has been enhanced because the magnetic field mitigates its effect on buoyancy force. Nanoparticles provide conduction regime, increase and maintenance the rate of heat transfer all over the cavity. Convection regime in $C2$ dominates the cavity but the inclination angle supplies conduction regime because the effect of buoyancy force is weaker than other cases. The convenient reason is the qualitative conversion of the stream which became symmetry as a result of energy consumed division into two parts. So any symmetry in isotherms implies to enhancement of conduction regime as seen in $C3$. $C4$ is as same as C2 but has large scalability to heat transfer. The insulated region (the bottom half of the right side) has not effect so the adiabatic condition obviously appears in the opposite side.

Fig. 2b shows the variation of local Nusselt number. The curve of $C1$ is symmetry around the centerline shaping a parabola; its head in the bottom and it is open up, i.e. the rate decreases in the left-half and increases in the right-half. $C2$ is decreasing curve, $C3$ is increasing, $C4$ is decreasing and tends to linearity, and $C5$ corresponds to $C3$. When $\Phi = \pi/2$, $C2$ and $C5$ have partial symmetry, $C4$ becomes totally symmetric, and $C1$, $C3$ are correspondent. Fig. 5 ensures that angle's effect differs w.r.t. the configurations, consequently it confirms boundary condition changing has the greatest effect on results and deductions.

(b) Effect of Hartmann and Rayleigh numbers

The core of circulating cell of stream lines in $C1$ moves toward bottom because the magnetic force reversely works at the V-diffusion's trend. Increase of Ha provides the conduction regime for $C1$ and decreases magnitude of stream function for $C2$ (Fig. 3a). The stream values multiply 100 times in $C1$. As Ra increases in $C4$, the left circulating cell tends to domination (Fig. 3b).

The rate of local heat transfer for $C1$ identify with $C3$ where they are symmetry around centerline shaping parabola its head is in bottom (Fig. 3c). $C2$ and $C4$ (tends to linearity) are decreasing

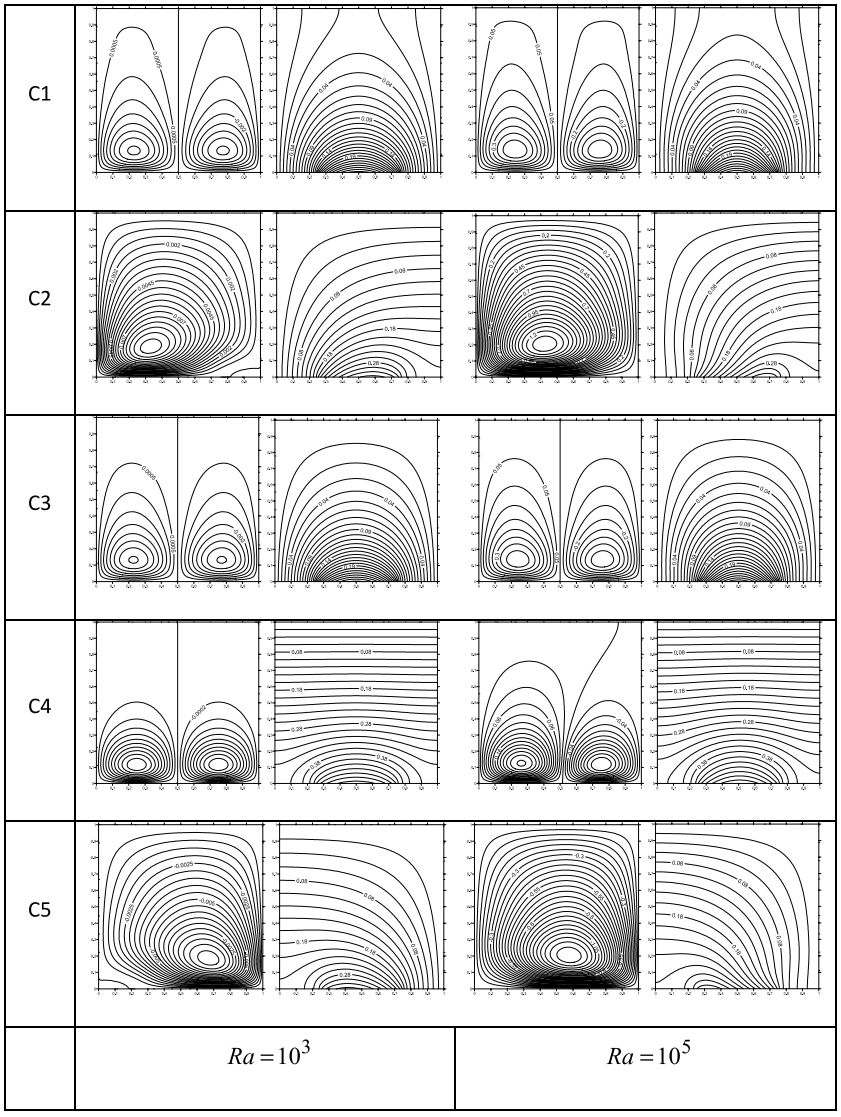

Fig. 3b. Streamlines (left) and Isothermal (right) at $\Phi = 0^0$, $\phi = 0.05$, $D = 0.5$, $B = 0.5$, $Ha = 50$.

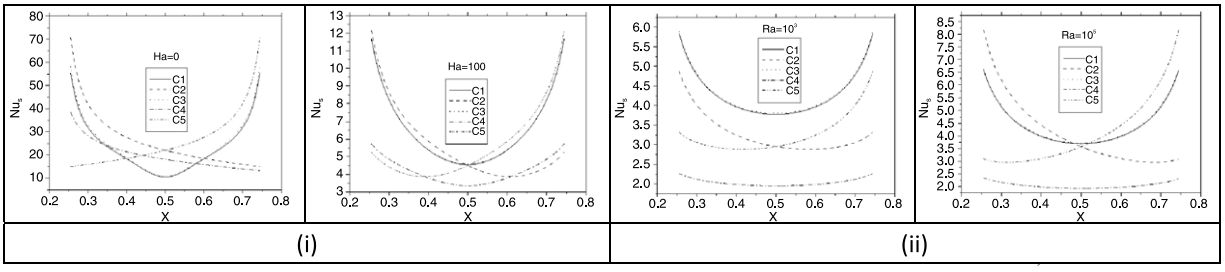

Fig. 3c. Profiles of the Local Nusselt number along the heat source (i) Ra $= 10^6$, $\Phi = \pi/2$, (ii) Ha $= 50$, $\Phi = 0$ at $\phi = 0.05$, $D = 0.5$, $B = 0.5$.

curves while $C5$ is increasing curve. The rate decreases generally at Ha $=$ 100, $C1$ relatively increase over than $C4$ which becomes symmetric curve too. $C4$ is more splaying than $C1$.

(c) Effect of solid volume fraction

Increase of φ provides conduction regime in $C1$ (Fig. 4a), where $\varphi = 0.1$ has the greatest value and increases the average of temperatures in $C2$. There is a radical difference between pure and nano cases in $C4$. Three circulating cells are found due to conduction regime in some regions (bottom, mostly) and convection style (top) where the insulated boundary surfaces. Perhaps the discrete cold regions on the boundaries help formation of the secondary cells.

$C1$'s profile of Nusselt number is symmetric (Fig. 4b) and $C3$ too. $C4$ is symmetry (as parabola) and its splaying is larger than $C1$ but has lower values than $C1$. It is found that $C3{\cdot}C2$ (decreasing curves) and $C5$ (increasing curve) are reciprocal and partial symmetric curves.

Curves of $\mathrm{Nu}_m - \Phi$ are symmetry around $\pi/2$ because magnetic field in interval $[\pi/2, \pi]$ plays the same role as before provided that inversion of the direction (Fig. 5). *C1, C2, C3* have one tip, $C4$ and $C5$ have two tips. The highest heat transfer rate is described

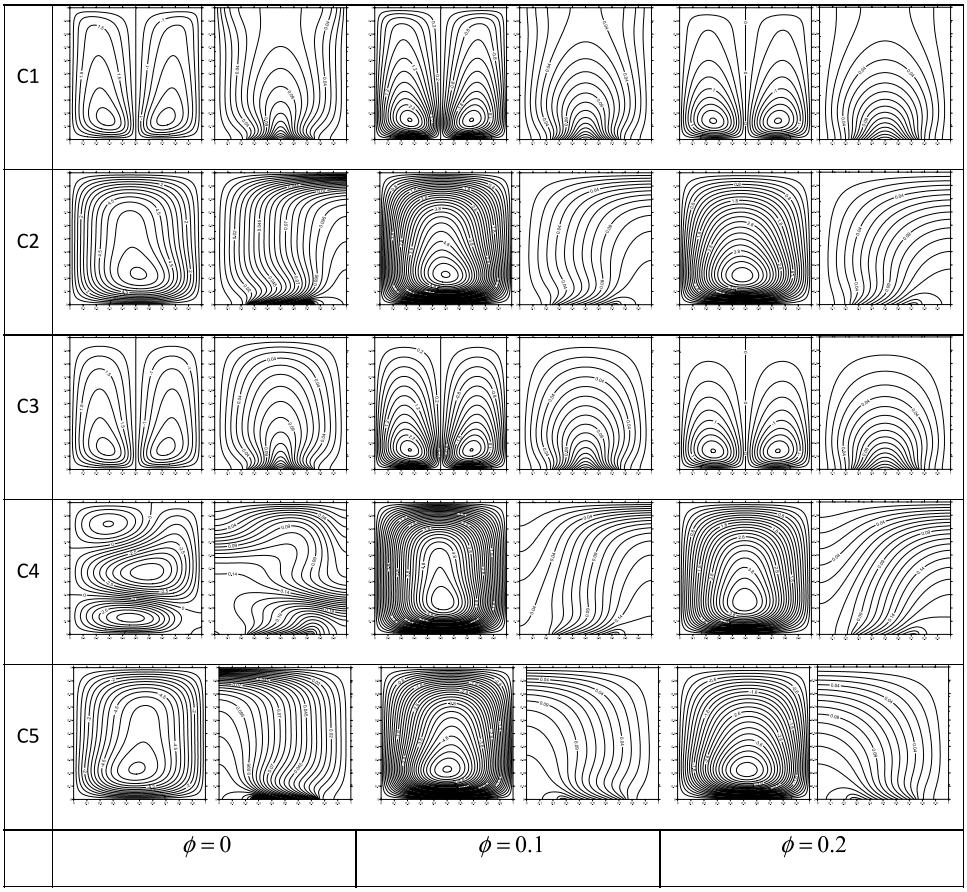

Fig. 4a. Streamlines(left) and Isothermal(right) at $\Phi = 0^0$, $Ra = 10^6$, $D = 0.5$, $B = 0.5$, $Ha = 50$.

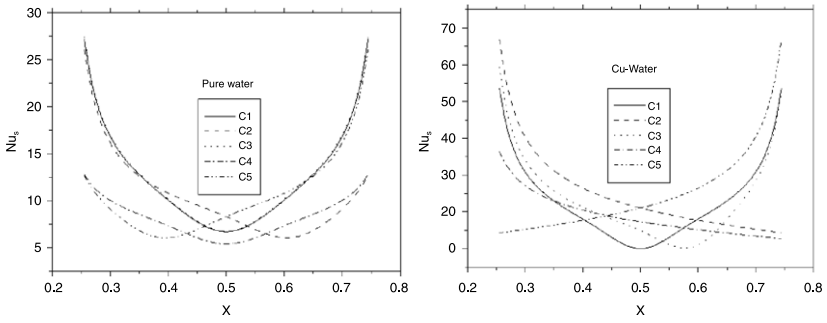

Fig. 4b. Profiles of the Local Nusselt number along the heat source $\phi = 0$, $Ra = 10^6$, $Ha = 50$, $D = 0.5$, $B = 0.5$, $\Phi = \pi/2$.

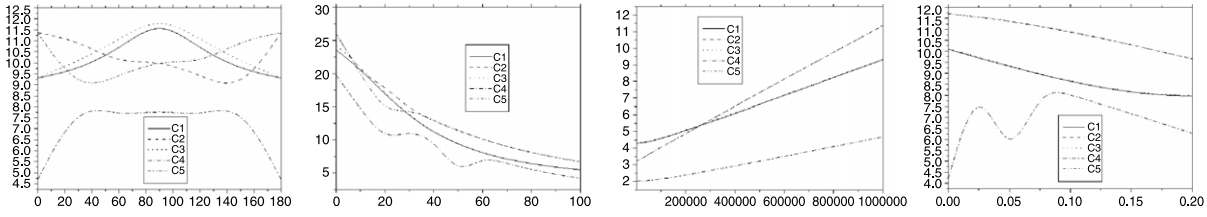

Fig. 5. Average Nusselt number with (i) Φ, (ii) Ha, (iii) Ra, (iv) φ (left to right) at $\phi = 0.05$, $Ra = 10^6$, $D = 0.5$, $Ha = 50$, $\Phi = 0°$.

by $C3$ while $C4$ enrolls the least. Dependence of average Nu on ϕ affects with boundary conditions of study case (Fig. 5), for example; $\{C1, C2, C3, C5\}$ are regular decreasing curves while C4, that has the least rates, is irregular, increasing in somewhere and decreasing in others.

Starting and finishing points are identical in pure case for following curves:

$\{C1, C2, C3\}$ have the same starting point and $\{C1, C3, C5\}$ have the same end point which is (27.5). $\{C4, C5\}$ have the same start point and $\{C2, C4\}$ which is (12.5). This means that the thermal emission at ends of heat source–sink is constant when boundary conditions change. Profile of $C1$ is symmetric around centerline and has the least rates for nanofluid while $C5$, which is increasing, has the highest rates. $C2$ curve is decreasing and $C4$

is less than it. $C3$ curve is symmetric but not around centerline. The relation between average Nu and Ha is decreasing globally (Fig. 5), some are regular and the others are irregular. $C4$ represent the lowest rates while $C5$ is the highest. The curves $C2$, $C3$, $C5$ match for Ha greater than 40. At 10^3, $C1$ and $C3$ are symmetric, correspondent parabola curves and enrolled the highest values. $C2$ (decreasing curve) and C5 (increasing curve) are reciprocal. $C4$ is symmetric, has very large splaying (closes to straight line) and enrolls the least heat transfer rates. $C1$ and $C3$ stay without change except for their relatively reduce in magnitude comparing to the others at 10^5. $C2$ and $C5$ hold the highest rates (Fig. 5). The relation of average Nu and Ra is globally increasing and linear as shown in Fig. 5. Both of $\{C1, C3\}$ and $\{C2, C5\}$ are correspondent and $C4$ enrolls the lowest rates.

5. Conclusion

A numerical simulation of MHD natural convection flows in a square cavity partially heated from below using Cu–water nanofluid has been studied for specified thermal boundary conditions at the top and sidewalls. The most important things has been reached are listed in following:

- Stream values decrease for nanofluid due to the heterogeneity of the particles.
- Fluid flow is symmetric around a vertical centerline in $C1$.
- $C2$ configuration rises stream values and vanishes the symmetry.
- All cases at $\Phi = \pi/2$ are symmetry due to the magnetic force divides the resultant force into two parts.
- Existence of adiabatic surfaces in the top helps to transfer temperature all over the cavity.
- As angle increases, the convection regime has been enhanced because the magnetic field mitigates its effect on buoyancy force.
- $C4$ is as same as $C2$ but has large scalability to heat transfer.
- The highest heat transfer rate is described by $C3$ while $C4$ enrolls the least.
- Increase of Ha provides the conduction regime for $C1$ and decreases magnitude of stream function for $C2$.
- The relation between average Nu and Ha is decreasing globally.
- The relation of average Nu and Ra is globally increasing and linear.
- Radical difference is found between pure and nano cases in $C4$.

References

Ahmad, T., Plee, S.L., Myers, J.P., 2010. FLUENT Theory Guide. ANSYS Inc.

Al-Najem, N.M., Khanafer, K.M., EL-Refaee, M.M., 1998. Numerical study of laminar natural convection in titled enclosure with transverse magnetic field. Int. J. Numer. Method. H. 8, 651–673.

Aydin, O., Yang, W.J., 2000. Natural convection in enclosures with localized heating from below and symmetrical cooling from sides. Internat. J. Numer. Methods Heat Fluid Flow 10 (5), 519–529.

Ben Cheikh, Nader, Ben Beya, Brahim, Lili, Taieb, 2007. Influence of thermal boundary conditions on natural convection in square enclosure partially heated from below. Int. Comm. Heat Mass Transfer 34, 369–379.

Brinkman, H.C., 1952. J. Chem. Phys. 20, 571.

Calgagni, B., Marsili, F., Paroncini, M., 2005. Natural convective heat transfer in square enclosures heated from below. Appl. Therm. Eng. 25, 2522–2531.

Einstein, A., 1956. Investigation on the Theory of Brownian Motion. Dover, New York.

El Jery, Atef, Hidouri, Nejib, Magherbi, Mourad, Ben Brahim, Ammar, 2010. Effect of an external oriented magnetic field on entropy generation in natural convection. Entropy 12, 1391–1417.

Ghasemi, B., Aminossadati, S.M., Raisi, A., 2011. Magnetic, field effect on natural convection in a nanofluid-filled square enclosure. Int. J. Thermal Sci. 50, 1748–1756.

Grosan, T., Revnic, C., Pop, I., Ingham, D.B., 2009. Magnetic field and internal heat generation effects on the free convection in a rectangular cavity filled with a porous medium. Int. J. Heat Mass Transfer 52, 1525–1533.

Haajizadeh, M., Ozguc, A.F., Tien, C.L., 1984. Natural convection in a vertical porous enclosure with internal heat generation. Int. J. Heat Mass Transfer 27, 1893–190.

Hamad, M.A.A., 2011. Analytical solution of natural convection flow of a nanofluid over a linearly stretching sheet in the presence of magnetic field. Int. Commun. Heat Mass Transfer 38, 487–492.

Heris, S.Z., Esfahany, M.N., Etemad, S.G., 2007. Experimental investigation of convective heat transfer of Al_2O_3/water nanofluid in circular tube. Int. J. Heat Fluid Flow 28, 203–210.

Ikezoe, Y., Hirota, N., Sakihama, T., Mogi, K., Uetake, H., Homma, T., Nakagawa, J., Sugawara, H., Kitazawa, K., 1998. Acceleration effect of the rate of dissolution of oxygen in a magnetic field. J. Jpn. Inst. Appl. Magnet. 22, 821–824.

Kalteh, M., Abbassi, A., Saffar-Avval, M., Harting, J., 2011. Eulerian-Eulerian two-phase numerical simulation of nanofluid laminar forced convection in a microchannel. Int. J. Heat Fluid Flow 32, 107–116.

Khanafer, K., Vafai, K., Lightstone, M., 2003. Buoyancy-driven heat transfer enhancement in a two-dimensional enclosure utilizing nanofluids. Int. J. Heat Mass Transfer 46, 3639–3653.

Lotfi, R., Saboohi, Y., Rashidi, A.M., 2010. Numerical study of forced convective heat transfer of nanofluids: comparison of different approaches. Int. Commun. Heat Mass Transf. 37, 74–78.

Mahmoudi, Amir Houshang, Pop, Ioan, Shhi, Mina, Talebi, Farhad, 2013. MHD natural convection and entropy generation in a trapezoidal enclosure using Cu-water nanofluid. Comput.& Fluids 27, 46–62.

Maiga, S.E.B., Nguyen, C.T., Galanis, N., Roy, G., 2004. Heat transfer behaviours of nanofluids in a uniformly heated tube. Superlattices Microstruct. 35, 543–557.

Maxwell, J., 1904. A Treatise on Electricity and Magnetism, second ed. Oxford University Press, Cambridge, UK.

Nemati, H., Farhadi, M., Sedighi, K., Ashorynejad, H.R., Fattahi, E., 2012. Magnetic field effects on natural convection flow of nanofluid in a rectangular cavity using the Lattice Boltzmann model. Sci. Iranica 19 (2), 303–310.

Oztop, H.F., Abu-Nada, E., 2008. Int. J. Heat Fluid Flow 29, 1326.

Ramos, R.A.V., Milanez, L.F., 1998. Numerical and experimental analysis of natural convection in cavity heated from below. In: Proceedings of 11th IHTC, vol. 3, Kyongju, Korea.

Rudraiah, N., Venkatachalappa, M., Subbaraya, C.K., 1995. Combined surface tension and buoyancy-driven convection in a rectangular open cavity in the presence of a magnetic field. Int. J. Nonlinear Mech. 30, 759.

Saidur, R., Leong, K.Y., Mohammad, H.A., 2011. A review on applications and challenges of nanofluids. Renew. Sustain. Energy Rev. 15, 1646–1668.

Sarkar, J., 2011. A critical review on convective heat transfer correlations of nanofluids. Renew. Sustain. Energy Rev. 15, 3271–3277.

Sarris, I.E., Lekakis, I., Vlachos, N.S., 2004. Natural convection in rectangular tanks heated locally from bellow. Int. J. Heat Mass Transfer 47, 3549–3563.

Sezai, I., Mohamad, A.A., 2000. Natural convection from a discrete heat source on the bottom of a horizontal enclosure. Int. J. Heat Mass Transfer 43, 2257–2266.

Sharif, M.A.R., Mohammad, T.R., 2005. Natural convection in cavities with constant flux heating at the bottom wall and isothermal cooling from the sidewalls. Int. J. Therm. Sci. 44, 865–878.

Sheikholeslami, M., 2014. Eur. Phys. J. Plus 248.

Sheikholeslami, M., Abdelman, S., Ganji, D.D., 2014. Numerical simulation of MHD nanofluid flow and heat transfer considering viscous dissipation. Int. J. Heat Mass Transfer 79, 212–222.

Sheikholeslami, M., Bandpy, M.G., Ellahi, R., Zeesham, A., 2014. Simulation of MHD CuO-water nanofluid flow and convective heat transfer considering Lorentz forces. J. Magn. Magn. Mater. 369, 69–80.

Sheikholeslami, M., Bandpy, M.G., Ganji, D.D., 2014. MHD free convection in an eccentric semi-annulus filled with nanofluid. J. Taiwan Inst. Chem. Eng. 45, 1204–1216.

Sheikholeslami, M., Bandpy, M.G., Ganji, D.D., 2014. Lattice Boltzmann method for MHD natural convection heat transfer using nanofluid. Powder Technol. 254, 82–93.

Sheikholeslami, M., Bandpy, M.G., Ganji, D.D., 2013. Numerical investigation of MHD effects on Al2O3-water nanofluid flow and heat transfer in a semi-annulus enclosure using LBM. Energy 60, 501–510.

Sheikholeslami, M., Bandpy, M.G., Ganji, D.D., 2014. Arab J. Sci. Eng. 39, 5007–5016.

Sheikholeslami, M., Bandy, M.G., Vajravelu, K., 2015. Lattice Boltzmann simulation of magnetohydrodynamic natural convection heat transfer of Al2O3-water nanofluid in a horizontal cylindrical enclosure with an inner triangular cylinder. Int. J. Heat Mass Transfer 80, 16–25.

Sheikholeslami, M., Ganji, D.D., 2014. Heated permeable stretching surface in a porous medium using Nanofluids. J. Appl. Fluid Mech. 7 (3), 535–542.

Sheikholeslami, M., Ganji, D.D., 2014. Numerical investigation for two phase modeling of nanofluid in a rotating system with permeable sheet. J. Molecular Liquids 194, 13–19.

Sheikholeslami, M., Ganji, D.D., 2014. Three dimensional heat and mass transfer in a rotating system using nanofluid. Powder Technol. 253, 789–796.

Sheikholeslami, M., Ganji, D.D., 2015. Nanofluid flow and heat transfer between parallel plates considering Brownian motion using DTM. Comput. Methods Appl. Mech. Engrg. 283, 651–663.

Sheikholeslami, M., Ganji, D.D., 2015. Entropy generation of nanofluid in presence of magnetic field using Lattice Boltzmann Method. Physica A 417, 273–286.

Sheikholeslami, M., Ganji, D.D., 2014. Ferrohydrodynamic and Magnetohydrodynamic effects on ferrofluid flow and convective heat transfer. Energy 75, 400–410.
Sheikholeslami, M., Ganji, D.D., Rashidi, M.M., 2014. Ferrofluid flow and heat transfer in a semi annulus enclosure in the presence of magnetic source considering thermal radiation. J. Taiwan. Inst. Chem. Eng. http://dx.doi.org/10.1016/j.jtice.2014.09.026.
Sheikholeslami, M., Gorji-Bandpy, M., 2014. Free convection of ferrofluid in a cavity heated from below in the presence of an external magnetic field. Powder Technol. 256, 490–498.
Sheikholeslami, M., Gorji-Bandpy, M., Ganji, D.D., 2012. Magnetic field effects on natural convection around a horizontal circular cylinder inside a square enclosure filled with nanofluid. Int. Comm. Heat Mass Transfer 39, 978–986.
Sheikholeslami, M., Gorji-Bandpy, M., Ganji, D.D., 2014. Soheil Soleimani, Heat flux boundary condition for nanofluid filled enclosure in presence of magnetic field. J. Molecular Liquids 193 (May), 174–184.
Sheikholeslami, M., Gorji-Bandpy, M., Ganji, D.D., Rana, P., Soleimani, Soheil, 2014. Magnetohydrodynamic free convection of Al2O3-water nanofluid considering Thermophoresis and Brownian motion effects. Comput. & Fluids 94 (1), 147–160.
Sheikholeslami, M., Gorji-Bandpy, M., Ganji, D.D., Soleimani, Soheil, 2014. Natural convection heat transfer in a cavity with sinusoidal wall filled with CuO-water nanofluid in presence of magnetic field. J. Taiwan Inst. Chem. Eng. 45 (1), 40–49.
Wakayama, N.I., 1991. Behavior of flow under gradient magnetic fields. J. Appl. Phys. 69, 2734–2736.
Wakayama, N.I., Okada, T., Okano, J., Ozawa, T., 2001. Magnetic promotion of oxygen reduction reaction with Pt catalyst in sulfuric acid solutions. Japan. J. Appl. Phys. 40, 269–271.
Wakayama, M., Wakayama, N.I., 2001. Magnetic acceleration of inhaled and exhaled flows in breathing. Japan. J. Appl. Phys. 40, 262–264.
Xuan, Y., Roetzel, W., 2000. Conceptions for heat transfer correlation of nanofluids. Int. J. Heat Mass Transfer 43, 3701–3707.